ARTICLE NO. 78-1127

Artificially Induced Boundary-Layer Transition on Blunt-Slender Cones at Hypersonic Speeds

A.H. Boudreau*
Sverdrup/ARO, Inc., Arnold Air Force Station, Tenn.

Research directed toward establishing criteria for distributed roughness-type boundary-layer trips on blunt-slender cones has been conducted at Mach numbers from 8 to 13. Results indicate that distributed roughness trips are superior to spherical-type trips in that equally effective distributed roughness trips are one-fifth as high and produce substantially smaller flowfield disturbances. Criteria are defined for optimum utilization of distributed roughness trips.

Nomenclature

k = trip element height, in.
M = Mach number
$N_{St,\infty}$ = Stanton number based on freestream conditions
P = pressure, psia
P_0' = freestream pitot pressure, psia
P_0 = reservoir pressure, psia
q_∞ = freestream dynamic pressure, psia
$\dot{q}$ = heat-transfer rate, Btu/ft^2-s
$\dot{q}_0$ = stagnation point heat-transfer rate, Btu/ft^2-s
Re_∞/ft = Reynolds number per foot based on freestream conditions
r_b, r_n = model base and nose radius, respectively, in.
s = surface distance along the model measured from the stagnation point, in.
T_w = model wall temperature, °R
T_∞ = freestream temperature, °R
T_{0_∞} = freestream total temperature, °R
x = axial distance along the model measured from the sharp apex, in.
δ = boundary-layer thickness at the trip
δ^* = boundary-layer displacement thickness
θ_c = cone half-angle, deg
ϕ = model circumferential angle, deg

Subscripts

e = boundary-layer edge conditions
k = at trip location
t = at the end of transition
∞ = freestream conditions

Introduction

EXPERIMENTALISTS resort to transition "fixing" by means of artificial tripping devices to match the turbulent boundary layers encountered in flight. Whereas a great many devices have been employed as boundary-layer trips, spheres of various sizes have generally become a standard with experimentalists. Spheres offer advantages, such as ease of application, uniformity of size, and accurate definability. However, the size of spherical trips (and other similar trips) required to trip the boundary layer has been known to be a strong function of Mach number, increasing rapidly as Mach number increases. This was pointed out some time ago by Potter and Whitfield[1] who noted that the ratio of trip height k to boundary-layer thickness δ_k (i.e., k/δ_k) "increases approximately as the first power of M_e at hypersonic Mach numbers" when transition is fixed at the tripping element. This means that in hypersonic flow the trip is usually as large as, or larger than, the boundary-layer thickness; therefore, the flowfield outside the boundary layer is disturbed as well. Usually, one can observe strong shock waves emanating from boundary-layer trips under hypersonic conditions. While experimentalists justify the use of such large trips by the requirements for turbulent boundary-layer similitude, flowfield analysts question the validity of test results when the flowfield disturbances are present. Sterrett et al.[2] have presented evidence that flowfield disturbances can be manifested far downstream of the tripping elements despite some indications that the boundary layer is turbulent and free of trip-induced anomalies. Their results are shown in Fig. 1, where the development of a hypersonic boundary layer on a flat plate is illustrated. The tripping elements (spheres, $k/\delta_k = 1.6$) produce noticeable anomalies in the boundary layer for approximately 20 sphere diameters downstream of the trips as shown by the oil flow photograph. Aft of that point (i.e., $20k$ downstream of the spheres) an apparently normal turbulent boundary layer is established judging from the oil flow photograph and heat-transfer rate measurements, which indicate a turbulent level. When a compression surface is encountered some $173k$ downstream of the trips, disturbances reappear in the boundary layer. This is remarkable considering that a separation region exists just forward of the wedge.

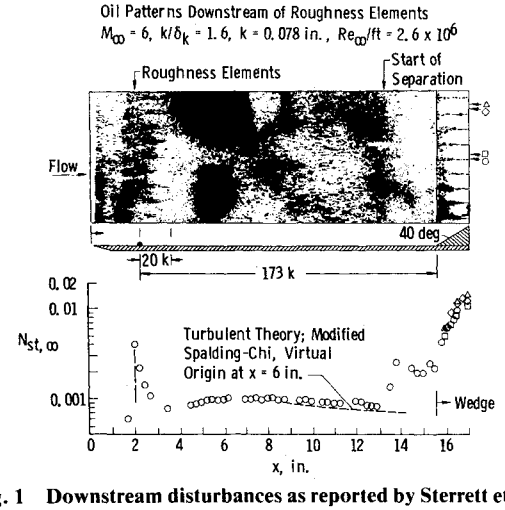

Fig. 1 Downstream disturbances as reported by Sterrett et al.[2]

Presented as Paper 78-1127 at the AIAA 11th Fluid and Plasma Dynamics Conference, Seattle, Wash., July 10-12, 1978; submitted Aug. 4, 1978; revision received Jan. 18, 1979.

Index categories: Boundary-Layer Stability and Transition; Supersonic and Hypersonic Flow.

*Project Engineer, Aerodynamics Projects Branch, von Kármán Gas Dynamics Facility.

It becomes obvious, therefore, that boundary-layer trips need to be reduced in size while maintaining their effectiveness. One method of achieving this is through the use of "distributed roughness" trips. This class of tripping device consists of tripping elements in close proximity to one another and extending over a relatively large area of the model. Examples of such trips are "grit-blasted surfaces," where the model is roughened by the impact of hardened steel grit air blasted onto the surface, and "distributed grit," where grit particules are bounded to the model with adhesives. Previous tests at the Arnold Engineering Development Center (AEDC) von Kármán Gas Dynamics Facility (VKF) have successfully employed grit-blasted surfaces and distributed grit to achieve turbulent boundary-layer flow on very blunt bodies. Also, unpublished data from AEDC/VKF Hypervelocity Wind Tunnel (F) (Tunnel F) have demonstrated that a 0.0035-in. peak-to-valley surface roughness could adequately trip the boundary layer on a hemisphere cylinder, as shown in Fig. 2. However, very little work has been done with distributed roughness on blunt-slender cones, the configuration of greatest practical interest in hypersonic testing today. The vast majority of tripping experiments have been carried out on flat plates, sharp cones, and hollow cylinders, as indicated by Pate.[3,4] Also, no systematic investigation has been conducted to date on distributed roughness as boundary-layer trips for wind tunnel testing. For these reasons the present study was instituted.

The experimental program consisted of entries in AEDC/VKF Hypersonic Tunnel B where Mach 8 data were obtained and in AEDC/VKF Tunnel F where Mach 13 data were obtained. This paper covers results from these tests.

Experimental Apparatus

Tunnels

Tunnel B is a Mach 6 or 8, closed-circuit, hypersonic wind tunnel with a 50-in.-diam test section.[5] Tunnel F is an arc-driven wind tunnel of the hotshot type[5,6] capable of providing Mach numbers from about 7 to 13 over a Reynolds-number-per-foot range from 0.20×10^6 to 50×10^6.

This Tunnel F test was conducted using the 48-in.-exit-diam contoured nozzle in the 54-in.-diam test section to obtain a nominal freestream Mach number of 12.5. Nitrogen was the test gas. Because of the relatively short (100 ms) test times, the model wall temperature remained essentially invariant from the initial value of approximately 540 °R; thus $T_w/T_{0_\infty} \cong 0.15$ to 0.25.

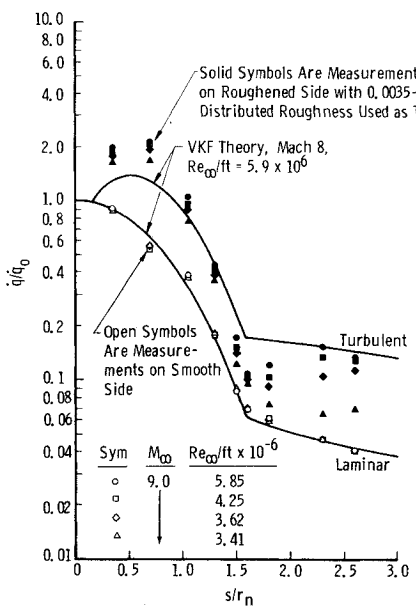

Fig. 2 Measured heat-transfer distribution on a 5-in.-diam hemisphere cylinder at Mach 9.

Model

The test article was a 7-deg half-angle cone with a sharp cone length of 48 in. This model, shown in Fig. 3, features ten interchangeable noses that provide sharp and blunt nose radii r_n of 0.295, 0.589, and 2.187 in. plus variations in the type of distributed roughness trips. The model was instrumented with up to 66 heat-transfer gages for both the Tunnel B and Tunnel F tests. The Tunnel F tests also included pressure measurements on the model. Twenty-three spherical trip rings were available at six model stations, providing several trip heights at each station. The sharp, 0.295-, and 0.589-in.-radius noses are shown in Fig. 4a. Examples of smooth (nominal 32-μ in. finish), applied grit, grit blasted, and numerically controlled machined (NCM) surfaces are shown. A blown up view of the 25-mil NCM nose is presented in Fig. 4b. Each tripping element is a pyramid with a total height (peak to valley) of 25 mils. The base plane of the pyramids is recessed $\frac{1}{3}$ k below the original unaltered model surface, as shown in Fig. 5. While these NCM noses are very durable, they are much more expensive than the applied grit on a smooth nose. Such NCM noses typically required 100 man-hours of machine shop work. The NCM noses were constructed of aluminum, whereas the model and the other noses shown in Fig. 4a were constructed from 1300 series stainless steel. The $r_n = 2.187$-in. nose is shown in Fig. 4c with 25-mil applied grit bonded to the surface. The distribution of grit in this photograph is typical of that used during the tests.

Instrumentation

Coaxial surface thermocouple gages were used to measure the surface heating rate distributions. In practical measurement applications the surface thermocouple behaves as a homogeneous, one-dimensional, semi-infinite solid. The instrument provides an electromotive force (EMF) directly proportional to surface temperature, which may be related by theory to the incident heat flux. All heat-transfer gages were bench calibrated prior to their installation into the model. The precision of these calibrations is estimated to be ±3%.

Procedures

Test Conditions

Nominal test conditions for the Tunnel B test were as shown in Table 1. Test conditions for Tunnel F are given in Table 2.

Test Procedures

The primary variables for the experiments in both Tunnels B and F were Reynolds number and trip configuration. Angle of attack was maintained at zero, and model wall temperature ratios (T_w/T_{0_∞}) remained relatively constant at 0.42 for Tunnel B and 0.15 to 0.25 for Tunnel F.

Test Conditions Uncertainty

Uncertainties in the basic tunnel parameters for Tunnel B have been estimated from repeat calibrations of P_0 and T_{0_∞}

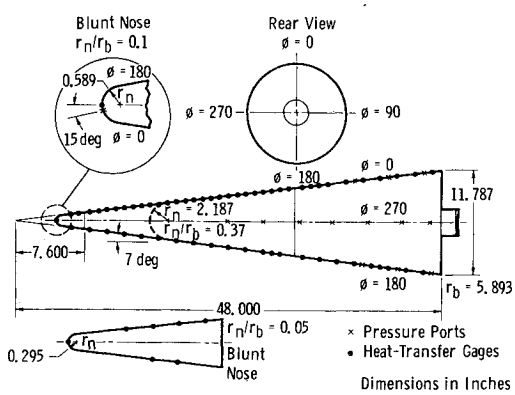

Fig. 3 Pressure/heat-transfer model (7-deg cone).

Table 1 Tunnel B test conditions

M_∞	P_0, psia	T_{0_∞} °R	q_∞, psi	p_∞, psi	T_∞, °R	$Re_\infty/\text{ft} \times 10^{-6}$
8.0	860	1343	3.94	0.088	97	3.75
8.0	770	1327	3.53	0.079	96	3.42
8.0	670	1323	3.09	0.069	96	3.00
8,0	614	1316	2.84	0.063	96	2.77
8.0	559	1324	2.57	0.058	96	2.49
8.0	446	1323	2.07	0.047	96	2.00

Table 2 Tunnel F test conditions

M_∞	P_0, psia	T_{0_∞} °R	q_∞, psi	p_∞, psi	T_∞, °R	$Re_\infty/\text{ft} \times 10^{-6}$
12.5	6800 to 15,500	2100 to 3500	5.7 to 9.5	0.04 to 0.10	88 to 126	3.0 to 6.0

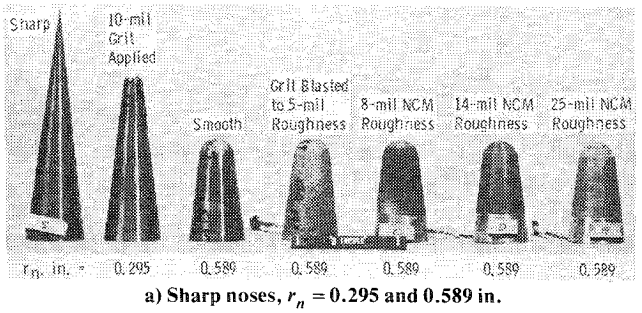

a) Sharp noses, $r_n = 0.295$ and 0.589 in.

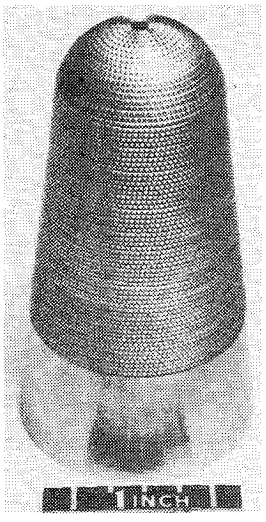

b) Blunt nose, $r_n = 0.589$ in., 25-mil NCM.

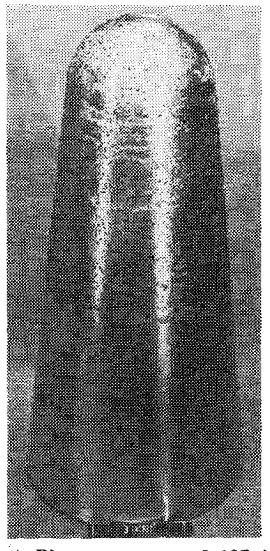

c) Blunt nose, $r_n = 2.187$ in., 25-mil grit.

Fig. 4 Photographs of 7-deg cone noses.

instruments and from the repeatability and uniformity of the tunnel flow during calibrations. These uncertainties are $M_\infty = \pm 0.3\%$, $P_0 = \pm 0.1\%$, $T_{0_\infty} = \pm 0.4\%$, $T_\infty = \pm 0.7\%$, $P_\infty = \pm 1.6\%$, and $Re_\infty/\text{ft} = \pm 1.1\%$.

For the Tunnel F tests, the uncertainties in measured data are higher because of the dynamics of the measurements and system errors. Representative values are $M_\infty = \pm 3\%$, $P_\infty = \pm 7\%$, $T_\infty = \pm 8\%$, and $Re_\infty/\text{ft} = \pm 11\%$.

Results and Discussion

Van Driest and Blumer[7] have presented an example of the effects of boundary-layer trips on the location of transition.

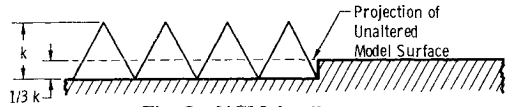

Fig. 5 NCM details.

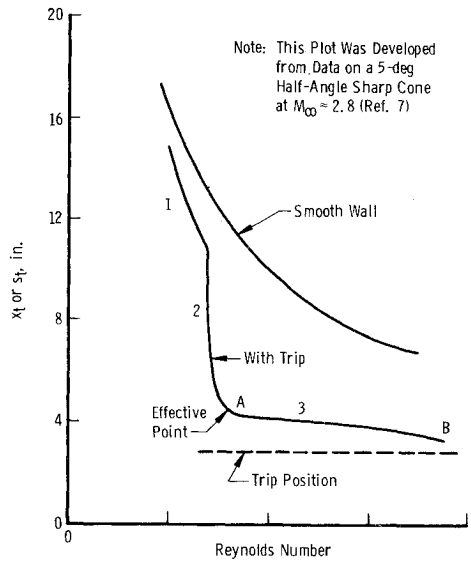

Fig. 6 Variation of x_t with unit Reynolds number.

Their example, shown in Fig. 6, plots the location of the end of transition (the point where fully turbulent flow exists) vs Reynolds number. Here x_t is the surface distance from a sharp nose to the end of transition and s_t is the blunt nose surface distance to the end of transition. In this example, x_t moves toward the nose of the cone in a continuous manner for the smooth wall case. For the tripped case, however, the forward movement of x_t is markedly different. Three distinct regions may be defined for the curve that represents the tripped case. In region 1 x_t is moved slightly forward by the trip; however, the transition location is primarily established by local flow conditions and freestream disturbances. This is essentially an area unaffected by the trips. Region 2 is characterized by a rapid forward movement of x_t for a correspondingly small change in Reynolds number until the point A is reached, which van Driest and Blumer have defined as the "effective point." In region 3 the roughness element is predominant in establishing the transition location (see Pate[3]), and further increases in Reynolds number yield only a gradual movement of transition toward the tripping element. For hypersonic conditions extremely high Reynolds numbers

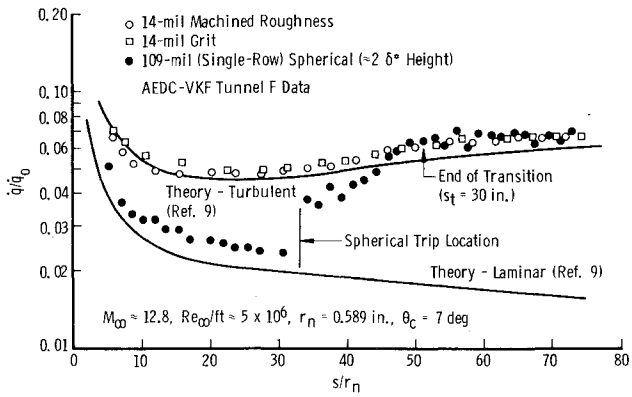

Fig. 7 Comparison of heat-transfer distribution on blunt cone using distributed roughness and spherical trips.

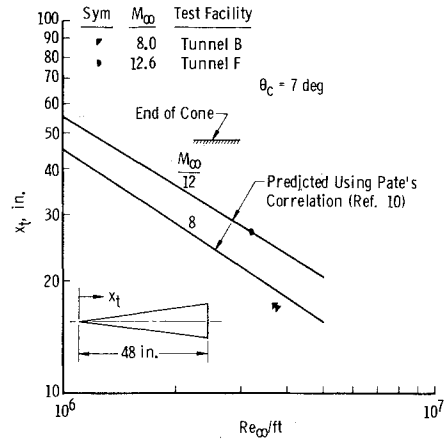

Fig. 8 Sharp cone natural transition results compared to Pate's correlation prediction.

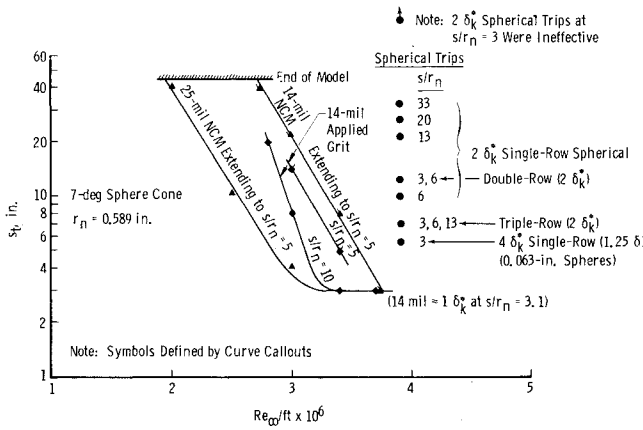

Fig. 9 Comparison of distributed roughness and spherical trips at Mach 8.

or extremely large trips may be required to bring x_t to the trip position, or near it (point B on the curve). The shape of the "tripped curve" in Fig. 6 and the location of the "effective point" are functions of the type and location of the tripping device used, as well as the type of body being considered.

The distance x_t or s_t may be determined by many methods. The experiments described herein used heat-transfer-rate measurements along the model surface to determine transition location. Early work in this area by Potter and Whitfield[1] has shown that the point at which the surface temperature (or heat-transfer rate) reaches a peak on a flat plate in supersonic flow corresponds to a point near the end of the transition region. More recently, Demetriades[8] compared various methods of transition detection on a 5-deg half-angle sharp cone at Mach 8 in AEDC/VKF Tunnel B. His results suggest that the peak heat-transfer rate on conical bodies at hypersonic velocities corresponds to the end of the transition zone, i.e., the area where fully turbulent flow is established. With these results in mind, the point at which a fully turbulent boundary layer is established will be defined as that point at which the heat-transfer rate reaches a peak or levels off to agree with turbulent theory after a rise from the laminar level. It is that point that we shall designate as x_t or s_t. This conclusion is well supported by a comprehensive review and correlation of transition location by Pate.[4] In determining x_t or s_t for the present tests, the experimental heat-transfer rates were compared to rates predicted by laminar and turbulent boundary-layer theory[9] as shown in Fig. 7. In this figure the distributed roughness data (open symbols) indicate a fully developed turbulent boundary layer over the entire body, whereas the spherical trips located at $s/r_n = 33$ yield a turbulent level at an s/r_n around 50, which corresponds to $s_t = 30$ in. The distributed roughnesses normally extended to $s/r_n = 5$ ($s = 3$ in. for the $r_n = 0.589$-in. nose); therefore, no valid data were available forward of 3 in.

In order to validate transition results per se, the 7-deg cone was tested both in Tunnel B and in Tunnel F with a sharp nose. The results are compared to prediction obtained using the well-known correlation of Pate[4,10] in Fig. 8. Good agreement is noted.

Basic results from the $r_n = 0.589$-in. nose on the 7-deg cone at Mach 8 are presented in Fig. 9. Here s_t (the surface distance to the end of transition) is plotted vs freestream unit Reynolds number. This figure compares the classical spherical trips with distributed roughness-type trips. Stainback[11] concludes that: "The laminar boundary layer can be tripped to produce turbulent flow on a blunt conical model and the values of the ratio of roughness height to boundary-layer displacement thickness k/δ_k^* required to accomplish this effect range from 1.7 to 2.2 when the roughness is located well downstream ($s/r_n = 13 \rightarrow 20$) from the spherical nose." He also noted that when $k/\delta_k^* = 2.7$ to 3.5, "a nonuniform circumferential heat-transfer rate is produced on the model downstream of the roughness element" for more than 20 in. Therefore, in the present tests, a single-row spherical trips spaced $4k$ apart and having a height $2\delta_k^*$ were placed at various s/r_n locations to determine what effects axial location might have. The results in Fig. 9 clearly indicate that one should place the trip around $s/r_n = 6$ for the present case. A $2\delta_k^*$ trip at $s/r_n = 3$ did not trip the boundary layer. This point will be discussed in more detail later in this paper in relation to both distributed roughness and spheres. A double row of $2\delta_k^*$ high spheres actually produced a slight rearward movement of s_t, although the difference is within the accuracy of measurement. Stainback[11] also found that a double row of spheres was essentially equivalent to a single row. When a triple row of $2\delta_k^*$ high trips was used, however, a 4-in. forward movement of s_t was noted, which was roughly equivalent to a single row of $4\delta_k^*$ high trips at $s/r_n = 3$. The $4\delta_k^*$ spheres (0.063-in. diam) and the triple row $2\delta_k^*$ spheres (0.025-, 0.063-, and 0.078-in. diam) are contrasted with the relatively small 14-mil distributed roughness results where s_t is at most 3 in. from the stagnation point at $\mathrm{Re}_\infty/\mathrm{ft} = 3.7 \times 10^6$. As noted previously, accurate measurements of heat-transfer rate were not obtained in the distributed roughness region; hence, $s_t = 3$ in. is the minimum determinable end of transition location. Note that the 14-mil NCM roughness and the 14-mil applied grit roughness results are essentially identical. One can, therefore, use either NCM roughness or applied grit as a distributed roughness trip with essentially equivalent results, on the basis of these trip configurations. While most of the distributed roughness trips extended to an s/r_n of 5, some data points were obtained with grit extending beyond that point. Note that by extending the grit to $s/r_n = 10$, a more effective trip is realized. Also shown in Fig. 9 are results from the 25-mil NCM nose, which indicate that the 7-deg cone model was tripped to fully turbulent flow

(i.e., $s_t = 3$ in.) at a freestream unit Reynolds number of only 3.2×10^6/ft.

The spherical trip results of Fig. 9 are further analyzed in Fig. 10 where the variation of the end of transition s_t with the ratio k/δ_k^* is compared to the correlation of Potter and Whitfield.[12] This correlation was developed from measurements on two-dimensional or axisymmetric bodies with negligible pressure gradients. Coats[13] when speaking about the Potter-Whitfield correlation (in regard to Coats' very blunt bodies) stated:

> A note of caution must be included regarding the validity of this or any two-dimensional correlation for bodies less blunt than those of the present investigation. The inviscid entropy layer discussed earlier may be a significant factor in the application of two-dimensional trip sizing techniques to such configurations. The very blunt noses of the present investigation produce thick entropy layers which are not believed to significantly affect either natural or induced boundary-layer transition, aside from the reduction in local Mach and unit Reynolds numbers; thus the two-dimensional techniques would be expected to be applicable. Conversely a slightly blunted body has a thin entropy layer with proportionally larger entropy gradients which must alter the boundary layer. Under these circumstances the two-dimensional techniques may not be applicable since they do not in any way account for the complicated flow resulting from absorption of the entropy layer by the boundary layer.

One should note, however, that the Potter-Whitfield method adequately predicts s_t and always yields a conservative answer. The experimental data of Fig. 10 indicate that a k/δ_k^* of 4 is required to bring s_t up to, or near, the trip. This differs with Stainback's conclusion that $k/\delta_k^* = 2$ is adequate for effective tripping. Evidently the criteria for effective tripping are more complicated than a mere δ_k^* criterion. As will be noted later, the pressure gradient has a significant influence on the trip size required, and Stainback's results were for $s_k/r_n = 13$ to 20 where the gradient is relatively small. An important advantage of the Potter-Whitfield method (in comparison to other correlations) is that s_t may be defined as any point between the natural transition location and the trip. If s_t is predefined, a trip size that is significantly smaller than that required for transition to occur at the trip may be determined. For instance, the experimental data indicate that by decreasing the spherical trip size from $k/\delta_k^* = 4$ to 2, the end of transition s_t moves back to a point 18 in. aft of the stagnation point. This may be satisfactory in many applications. Note also that the k/δ_k^* ratio for effective distributed roughness trips (when δ_k^* is taken at $s/r_n = 6.5$) is only 0.55 at this location.

Results from the 7-deg cone with nose radii r_n of 0.295 and 2.187 in. are compared to the $r_n = 0.589$-in. results in Fig. 11. Spherical trips placed at $s/r_n = 13$ yield essentially identical results for the $r_n = 0.295$ and 0.589-in. noses. The $r_n = 0.295$-in. transition location is 4 in. forward of the $r_n = 0.589$-in. location, but this is to be expected since the 0.063-in. trips used were $2.2\delta_k^*$ instead of $2.0\delta_k^*$. The distributed roughness results, however, indicate that the 0.295-in.-radius nose is much more sensitive to variations in unit Reynolds number. The large nose ($r_n = 2.187$ in.) results are indicated by open symbols and show that the large radius greatly aids the distributed roughness tripping. Grit was gradually removed from the stagnation region of the large nose in three steps in order to determine an optimum starting point for the distributed roughness. Note that the difference in s_t between the 10- and 45-deg starting points is only 0.6 in., whereas the difference between 45- and 65-deg points is more than twice that length. These data and other experience with the $r_n = 0.589$-in. nose tend to point to a 45-deg starting location as being close to optimum. This result seems logical since the 45-deg location also corresponds to the area of maximum local Reynolds number on a hemisphere nose.

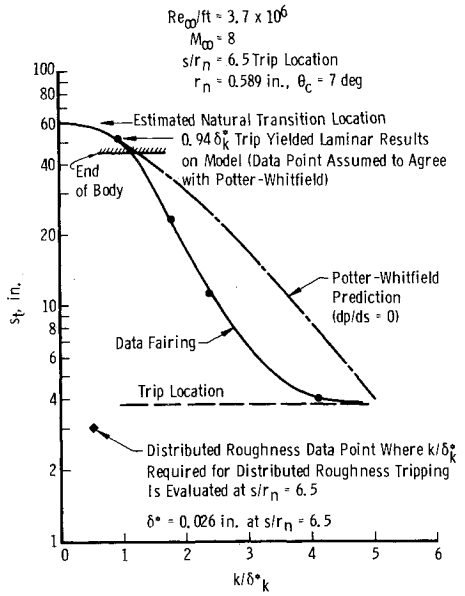

Fig. 10 Single-row spherical trip results compared to the Potter-Whitfield prediction.[12]

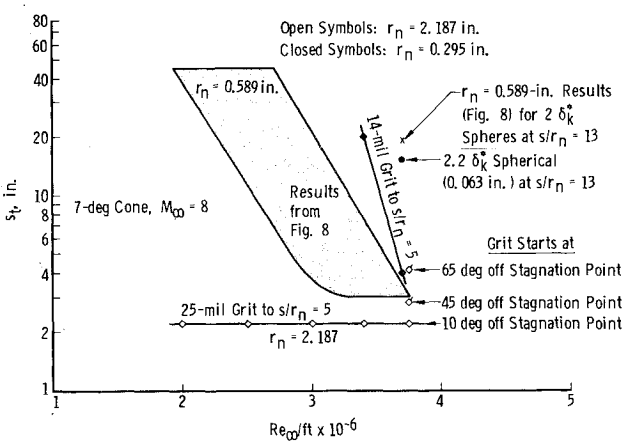

Fig. 11 Tripped transition location data obtained on the $r_n/r_b = 0.05$ and 0.37 bluntness cone configuration at Mach 8.

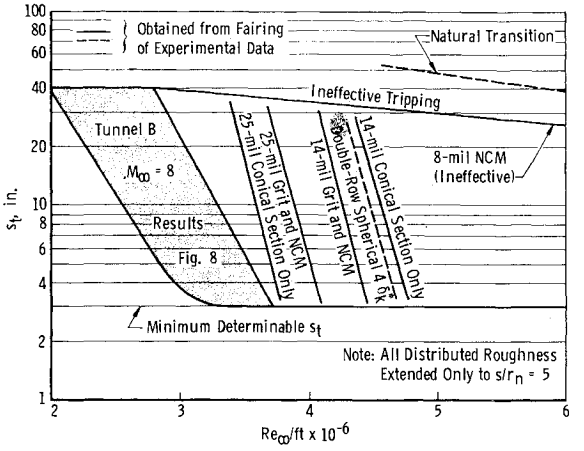

Fig. 12 Summary of tripped results at $M_\infty \approx 12.7$ ($r_n = 0.589$ in., 7-deg cone).

Tripping results at Mach 12.7 are presented in Fig. 12. Although the trends are similar to the Mach 8 results, one notes a shift to higher values of unit Reynolds number in order to achieve effective tripping. While such strong Mach number effects are well known for the case of spherical tripping, these data suggest that the Mach number effects on distributed-roughness-type trips are equally strong. This Mach number dependence is primarily due to the decrease of local pressure in the trip region as Mach number increases. Note that the double-row $4\delta_k^*$ high spherical trips (at $s/r_n = 3$ and 6) give results similar to the 14-mil distributed roughness trips, as was the case at Mach 8. The fairings marked "Conical Sec. Only" represent results from noses where grit was applied starting at approximately 75 deg from the stagnation point and extending to $s/r_n = 5$. The fact that these results agree with the other distributed roughness results (within data repeatability) indicates that the tripping effect of grit on the hemisphere section is much less important when compared to grit on the conical section. A run with applied 14-mil grit only on the hemisphere section of the nose produced results falling along the ineffective tripping line at a Reynolds number of 4.8×10^6/ft.

Having determined that the conical section of the $r_n = 0.589$-in. nose was most important for effective distributed roughness tripping, tests were conducted at Mach 8 to determine how far the grit should extend along the conical section. Figure 13 presents results on the $r_n = 0.589$-in. nose. Here the nondimensional surface distance to the end of transition, s_t/r_n is plotted against s/r_n at the end of the grit coverage. The results shown are, of course, a strong function of Reynolds number, and by varying Re_∞/ft one could generate a family of such curves. These results, however, do point out that the distributed roughness trip becomes more effective as the grit is extended rearward. Note that the end of transition reaches the end of the grit at approximately $s/r_n = 11.5$. By examining the pressure distribution along the surface (Fig. 14), one can observe that this roughly corresponds to the bottom of the commonly termed "pressure bucket," i.e., the area of minimum surface pressure.

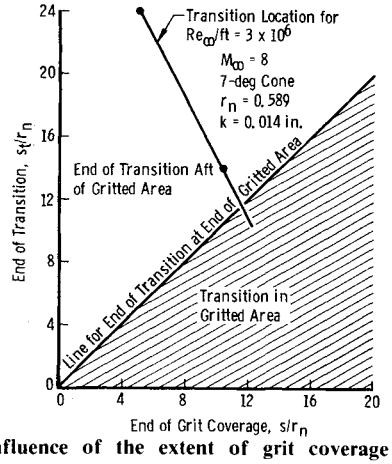

Fig. 13 Influence of the extent of grit coverage on transition location.

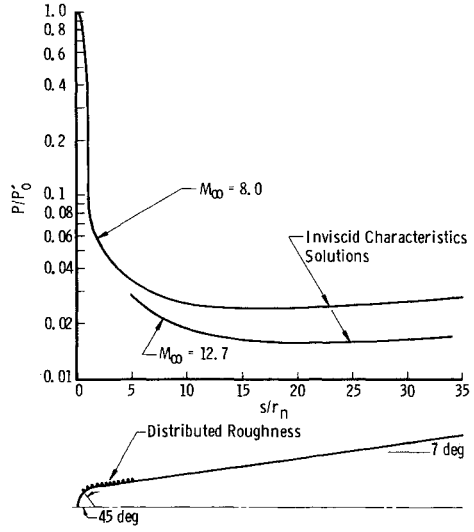

Fig. 14 Pressure distribution on the 7-deg sphere cone.

From the results presented thus far and by examining Fig. 14, one can gain insight into the behavior of the distributed roughness tripping mechanism. Optimum tripping is evidently obtained when one begins the roughness area at approximately 45 deg (as indicated by Fig. 11) and extends the roughness as far toward the bottom of the pressure bucket as practical (as shown in Fig. 13). Most of the distributed roughness results of the present study used roughness extending to $s/r_n = 5$, which, acording to Fig. 14, has a pressure 40% above the bucket value. As noted in Fig. 9, an advantage was seen in extending the grit to $s/r_n = 10$, which has a pressure within 10% of the bucket value.

To trip the boundary layer in the nose region of a blunted cone, one must contend with the strong favorable pressure gradient in that area. This pressure gradient tends to maintain the boundary layer in a laminar state and will actually "relaminarize" turbulence generated near the stagnation point. This can happen even when surface roughness is present, as shown by the data in Fig. 2 where, at an s/r_n of 1.6 or 1.8, the heat-transfer level drops from a previously turbulent value to a transitional value. The phenomenon has been termed "laminarization" by Launder and Jones[14] and has been observed for many years by experimentalists. Therefore, in order to trip the boundary layer, the trip size must increase relative to the boundary-layer thickness as one progresses toward the stagnation point from the "bucket"; i.e., the ratio of k/δ_k^* must increase in order to overcome the

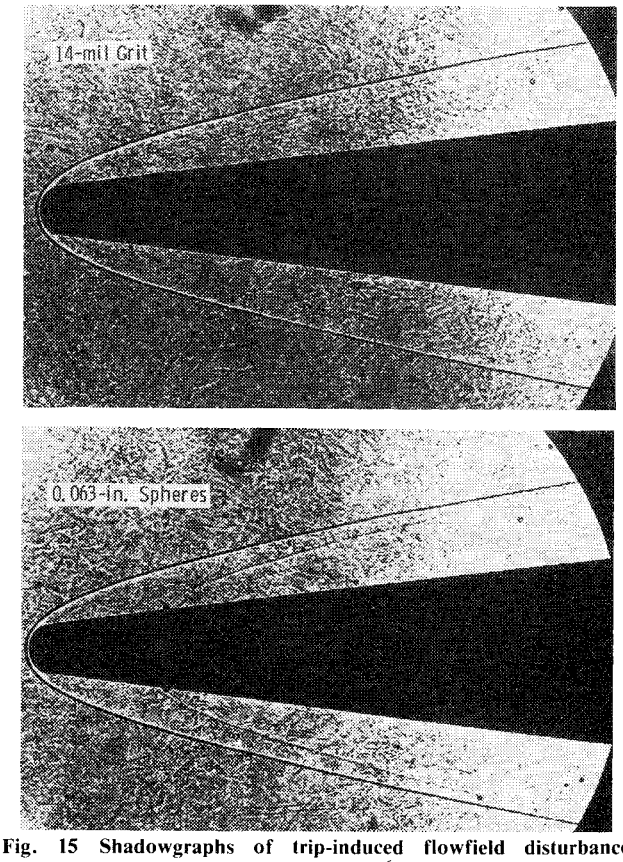

Fig. 15 Shadowgraphs of trip-induced flowfield disturbances ($M_\infty = 8$, $r_n = 0.589$ in., $Re_\infty/\text{ft} = 3.7 \times 10^6$).

expansion aft of the trip location. This conclusion is supported by the data of McCauley et al.,[15] who found that k/δ_k^*'s on the order of 25 were required for spherical trips located 45 deg off the stagnation point and that "k/δ_k^* effective" decreased as the trips were moved aft. As previously noted in Fig. 10, k/δ_k^* need be only 4 or less for effective spherical-type trips located at $s/r_n = 6.5$. Hence one cannot simply speak of trip size in terms of k/δ_k^*, especially when strong favorable pressure gradients are present. As previously mentioned, distributed roughness trips offer an advantage of much smaller sizes than spheres; however, the tripping mechanism must somewhat follow that of the spherical-type trips. The distributed roughness tripping elements in the forward section of the roughness area evidently trip the boundary layer since they have a relatively high ratio of k/δ_k^* at that point. This is caused by the displacement thickness being relatively thin on the nose section and increasing in thickness rapidly as the expansion progresses onto the conical section. After the initial tripping the relatively small roughness apparently "maintains" the turbulent state through the remainder of the expansion. As the strength of expansion increases because of either increasing Mach number or decreasing cone angle, the size of the distributed roughness (or the Reynolds number) must increase for effective tripping. Note in Fig. 14, for instance, that the expansion is substantially stronger at $M_\infty = 12.7$ than at $M_\infty = 8$.

The distributed roughness trip heights used in this current study varied from 8 to 25 mils. As previously stated, the 8-mil roughness proved to be ineffective at the Reynolds numbers encountered in these tests. Hence, for the case of Tunnel B or Tunnel F at $M_\infty \approx 12.5$, roughnesses on the order of 14 to 25 mils are required. The grit blasting technique consisted of air blasting hardened steel particles onto the model surface to roughen it. To date, this technique has produced a surface roughness up to 6 mils. Attempts to achieve larger roughnesses via larger particles, model material variations, and higher air delivery pressures have been unsuccessful. Therefore, the experimentalist should consider distributed roughness produced by grit blasting only if the required trip height k is equal to or less than 6 mils.

Evidence that distribute roughness trips produce relatively small disturbances (shock waves) in the flowfield compared to equally effective spherical trips is demonstrated by the shadowgraph photographs of Fig. 15. Here, 14-mil applied grit and $4\delta_k^*$ high (0.63-in.) spherical trips are compared at identical test conditions. A series of shock waves emanating from the grit is barely visible in the upper photograph, and they are relatively weak in comparison to the shock wave produced by the spheres. One should recall that the distributed roughnesses applied for tripping purposes here are comparable to the roughness encountered on some flight vehicles.

Conclusions

Research directed at establishing criteria for distributed-roughness-type boundary-layer trips has been conducted and the following conclusions may be drawn from this work:

1) Sharp cone untripped (natural) transition data compare very well with Pate's correlation and lend credibility to the blunt nose results.

2) Single rows of spherical trips should be placed slightly forward of the "pressure distribution bucket" and should be from $2\delta_k^*$ to $4\delta_k^*$ high for effective tripping. The $4\delta_k^*$ value brings transition near the trip.

3) Triple rows of $2\delta_k^*$ high spherical trips perform as well as a single row of $4\delta_k^*$ high trips.

4) Spherical trip results on blunt-slender cones are in fair agreement with the Potter-Whitfield prediction technique.

5) Distributed roughness trips one-fifth the height of spherical trips yield excellent results while producing substantially less disturbance to the flowfield, as determined by shadowgraph photographs.

6) Distributed roughness applications on blunt-slender cones should start 45 deg off the stagnation point and extend up the "pressure bucket," or as close to it as practical.

7) As with spherical-type trips, the distributed-roughness-type trip effectiveness is a strong function of Mach number.

Acknowledgments

The research reported herein was performed by the Arnold Engineering Development Center, Air Force Systems Command. Work and analysis for this research was done by personnel of ARO, Inc., a Sverdrup Corporation Company, operating contractor of AEDC. Further reproduction is authorized to satisfy needs of the U.S. Government.

References

[1] Potter, J.L. and Whitfield, J.D., "Effects of Slight Nose Bluntness and Roughness on Boundary Layer Transition in Supersonic Flows," *Journal of Fluid Mechanics,* Vol. 12, 1962, Pt. IV, pp. 501-535.

[2] Sterrett, J.R., Morrisette, E.L., Whitehead, A.H. Jr., and Hicks, R.M., "Transition Fixing for Hypersonic Flow," NASA TN D-4129, Oct. 1967.

[3] Pate, S.R., "Supersonic Boundary Layer Transition: Effects of Roughness and Freestream Disturbances," *AIAA Journal,* Vol. 9, May 1971, pp. 797-803.

[4] Pate, S.R., "Dominance of Radiated Aerodynamic Noise on Boundary-Layer Transition in Supersonic-Hypersonic Wind Tunnels: Theory and Application," Ph. D. Dissertation, Univ. of Tennessee, Knoxville, March 1977.

[5] "von Kármán Gas Dynamics Facility," *Test Facilities Handbook,* 10th Ed., Vol 3, Arnold Engineering Development Center, May 1974.

[6] Pate, S.R. and Eaves, R.H. Jr., "Recent Advances in the Performance and Testing Capabilities of the AEDC-VKF Tunnel F (HOTSHOT) Hypersonic Facility," AIAA Paper 74-84, presented at the AIAA 12th Aerospace Sciences Meeting, Washington, D.C., Jan. 30-Feb. 1, 1974.

[7] Van Driest, E.R. and Blumer, C.B., "Boundary Layer Transition on Cones and Spheres at Supersonic Speeds – Effects of Roughness and Cooling," Ocean Systems Operations of North American Rockwell Corp., Anaheim, Calif., AFOSR Scientific Rept. 67-2048, July 1967.

[8] Demetriades, A., "Hydrodynamic Stability and Transition to Turbulence in the Hypersonic Boundary Layer Over a Sharp Cone," AFOSR-TR-75-1435 (ADA016536), July 1975.

[9] Mayne, A.W. Jr. and Dyer, D.F., "Comparison of Theory and Experiment for Turbulent Boundary Layers on Simple Shapes at Hypersonic Conditions," *Proceedings of the 1970 Heat-Transfer and Fluid Mechanics Institute,* Stanford University Press, 1970, pp. 168-188.

[10] Pate, S.R., "Measurements and Correlations of Transition Reynolds Numbers on Sharp Slender Cones at High Speeds," AEDC-TR-69-172 (AD698326); also *AIAA Journal,* Vol. 9, June 1971, pp. 1082-1090.

[11] Stainback, P.C., "Effect of Unit Reynolds Number, Nose Bluntness, Angle of Attack, and Roughness on Transition on a 5° Half-Angle Cone at Mach 8," NASA TN D-4961, Jan. 1969.

[12] Potter, J.L., and Whitfield, J.D., "Boundary-Layer Transition under Hypersonic Conditions," AEDC-TR-65-99 (AD462716), May 1965; presented at AGARD Specialists' Meeting on Recent Developments in Boundary Layer Research, Naples, Italy, AGARDograph 97, Pt. 3, May 1965.

[13] Coats, J.D., "Investigation of the Effects of Nose Bluntness on Natural and Induced Boundary-Layer Transition on Axisymmetric Bodies in Supersonic Flow," AEDC-TR-73-36 (AD755843), Feb. 1973.

[14] Launder, B.E. and Jones, W.P., "On the Prediction of Laminarization," Ministry of Technology Aeronautical Research Council, C.P. No. 1036, 1968.

[15] McCauley, W.D., Saydah, A., and Bueche, J., "The Effect of Controlled Three Dimensional Roughness on Hypersonic Laminar Boundary Layer Transition," *AIAA Journal,* Vol. 4, Dec. 1966, pp. 2142-2148.